LETTER

doi:10.1038/nature13883

Passive radiative cooling below ambient air temperature under direct sunlight

Aaswath P. Raman[1], Marc Abou Anoma[2], Linxiao Zhu[3], Eden Rephaeli[1] & Shanhui Fan[1]

Cooling is a significant end-use of energy globally and a major driver of peak electricity demand. Air conditioning, for example, accounts for nearly fifteen per cent of the primary energy used by buildings in the United States[1]. A passive cooling strategy that cools without any electricity input could therefore have a significant impact on global energy consumption. To achieve cooling one needs to be able to reach and maintain a temperature below that of the ambient air. At night, passive cooling below ambient air temperature has been demonstrated using a technique known as radiative cooling, in which a device exposed to the sky is used to radiate heat to outer space through a transparency window in the atmosphere between 8 and 13 micrometres[2–11]. Peak cooling demand, however, occurs during the daytime. Daytime radiative cooling to a temperature below ambient of a surface under direct sunlight has not been achieved[3,4,12,13] because sky access during the day results in heating of the radiative cooler by the Sun. Here, we experimentally demonstrate radiative cooling to nearly 5 degrees Celsius below the ambient air temperature under direct sunlight. Using a thermal photonic approach[14–25], we introduce an integrated photonic solar reflector and thermal emitter consisting of seven layers of HfO_2 and SiO_2 that reflects 97 per cent of incident sunlight while emitting strongly and selectively in the atmospheric transparency window. When exposed to direct sunlight exceeding 850 watts per square metre on a rooftop, the photonic radiative cooler cools to 4.9 degrees Celsius below ambient air temperature, and has a cooling power of 40.1 watts per square metre at ambient air temperature. These results demonstrate that a tailored, photonic approach can fundamentally enable new technological possibilities for energy efficiency. Further, the cold darkness of the Universe can be used as a renewable thermodynamic resource, even during the hottest hours of the day.

Consider a radiative cooler of area A at temperature T, whose spectral and angular emissivity is $\epsilon(\lambda,\theta)$. When the radiative cooler is exposed to a daylight sky, it is subject to both solar irradiance and atmospheric thermal radiation (corresponding to ambient air temperature T_{amb}). The net cooling power P_{cool} of such a radiative cooler is given by:

$$P_{cool}(T) = P_{rad}(T) - P_{atm}(T_{amb}) - P_{Sun} - P_{cond+conv} \quad (1)$$

In equation (1) the power radiated out by the structure is:

$$P_{rad}(T) = A\int d\Omega \cos\theta \int_0^\infty d\lambda I_{BB}(T,\lambda)\epsilon(\lambda,\theta) \quad (2)$$

Here $\int d\Omega = 2\pi\int_0^{\pi/2} d\theta \sin\theta$ is the angular integral over a hemisphere. $I_{BB}(T,\lambda) = \frac{2hc^2}{\lambda^5}\frac{1}{e^{hc/(\lambda k_B T)}-1}$ is the spectral radiance of a blackbody at temperature T, where h is Planck's constant, k_B is the Boltzmann constant, c is the speed of light and λ is the wavelength.

$$P_{atm}(T_{amb}) = A\int d\Omega \cos\theta \int_0^\infty d\lambda I_{BB}(T_{amb},\lambda)\epsilon(\lambda,\theta)\epsilon_{atm}(\lambda,\theta) \quad (3)$$

is the absorbed power due to incident atmospheric thermal radiation, and:

$$P_{Sun} = A\int_0^\infty d\lambda \epsilon(\lambda,\theta_{Sun})\, I_{AM1.5}(\lambda) \quad (4)$$

is the incident solar power absorbed by the structure. We arrive at equation (3) and equation (4) by using Kirchhoff's radiation law to replace the structure's absorptivity with its emissivity $\epsilon(\lambda,\theta)$. The angle-dependent emissivity of the atmosphere is given by[6]: $\epsilon_{atm}(\lambda,\theta) = 1 - t(\lambda)^{1/\cos\theta}$, where $t(\lambda)$ is the atmospheric transmittance in the zenith direction[26]. In equation (4), the solar illumination is represented by $I_{AM1.5}(\lambda)$, the AM1.5 spectrum. We assume the structure is facing the Sun at a fixed angle θ_{Sun}. Thus the term P_{Sun} does not have an angular integral, and the structure's emissivity is represented by its value at θ_{Sun}.

$$P_{cond+conv}(T,T_{amb}) = Ah_c(T_{amb} - T) \quad (5)$$

is the power lost due to convection and conduction. $h_c = h_{cond} + h_{conv}$ is a combined non-radiative heat coefficient that captures the collective effect of conductive and convective heating owing to the contact of the radiative cooler with external surfaces and air adjacent to the radiative cooler.

Equation (1) in general relates the cooling power $P_{cool}(T)$ of the surface, that is, the net power outflow of the surface, as a function of its temperature. Such a surface becomes a daytime cooling device if there is a net positive power outflow when $T = T_{amb}$ under direct sunlight, that is, if it radiates more heat out to space than it gains by absorbing sunlight and atmospheric thermal radiation. The power outflow $P_{cool}(T = T_{amb})$ then defines its cooling power at ambient air temperature. In the absence of net outflow, a radiative cooler's temperature should reach a steady-state temperature below ambient. The solution of equation (1) with $P_{cool}(T) = 0$ defines the steady-state temperature T_s. The goal of our experiment is to demonstrate a daytime radiative cooling device with $T_s < T_{amb}$, and to measure its cooling power as a function of T under direct sunlight, corresponding to peak daytime conditions.

To achieve daytime radiative cooling, the device must satisfy a very stringent set of constraints as dictated by the power balance equation of equation (1). First, it must reflect sunlight strongly to minimize P_{Sun}. Therefore, it must be strongly reflecting over visible and near-infrared wavelength ranges. Second, it must strongly emit thermal radiation P_{rad} while minimizing incident atmospheric thermal radiation P_{atm} by minimizing its emission at wavelengths where the atmosphere is opaque. Thus, the device must emit selectively and strongly only between 8 μm and 13 μm, where the atmosphere is transparent, and reflect at all other wavelengths. These constraints are formidable and fundamentally thermodynamic in nature. Radiative power scales as T^4, and the Sun, at 5,777 K, far outstrips the radiation of room-temperature objects on Earth, which are typically around 300 K. Even with an ideally selective emitter that emits only in the atmospheric transparency window, over 90% of incident sunlight must be reflected to remain at ambient temperature. In practice, to achieve meaningful daytime radiative cooling more than

[1]Ginzton Laboratory, Department of Electrical Engineering, Stanford University, Stanford, California 94305, USA. [2]Department of Mechanical Engineering, Stanford University, Stanford, California 94305, USA. [3]Department of Applied Physics, Stanford University, Stanford, California 94305, USA.

94% of sunlight must be reflected, especially given variation in atmospheric conditions across different geographic regions[27]. This is particularly challenging when combined with the goal of emitting strongly and selectively in the atmospheric window. Previous approaches using metallic reflectors and conventional thermal emitters with reflective cover foils have thus proved to be insufficient to achieve cooling under direct sunlight. Finally, the radiative cooler must be well sealed from its environment to minimize h_c and in turn $P_{cond+conv}$. This constraint presents an experimental design challenge during the daytime given that most surfaces that might be in contact with the radiative cooler will themselves heat up when exposed to sunlight and transfer this added heat to the cooler.

A previous paper presented a theoretical design of a photonic structure capable of satisfying the emission and reflection requirements for cooling[14]. The design there involved the use of a complex two-dimensional photonic crystal that would require photolithography. Here we introduce and numerically optimize an alternative theoretical design based on one-dimensional photonic films that is more amenable to large-scale fabrication, and experimentally realize it. Furthermore, we design and build an apparatus that minimizes heat load on the radiative cooler, allowing us to observe below-ambient cooling in the daytime for the first time.

The rooftop measurement apparatus that minimizes h_c, and is used to experimentally demonstrate radiative cooling under direct sunlight, is shown in Fig. 1a. The design of the apparatus, shown schematically in Fig. 1b and c, reduces both convection and conduction to the radiative cooler under peak solar irradiance. The radiative cooling surface, deposited on a 200-mm silicon wafer, is placed on a polystyrene pedestal which is supported by a clear acrylic box (see Methods for details). A clear 12.5-μm polyethylene film lies above the sample as an infrared-transparent wind shield. As can be seen in the two-dimensional schematic of the apparatus in Fig. 1c, the radiative cooler is thus suspended in a relatively well-sealed air pocket. Such an air pocket design represents a key innovation in the experimental demonstration of daytime radiative cooling: note that our sample is far smaller than the surrounding roof. This design aims to ensure that any surface in immediate contact with the air pocket or the sample will heat up minimally due to solar irradiance. Finally, to ensure peak sunlight irradiance of up to 890 W m^{-2} on the radiative cooler during the winter months in which testing was conducted, the entire apparatus is tilted 30° towards the south. This experimental constraint reduces sky access for the purposes of thermal radiation, so for the same setup, better cooling performance would be expected if one were to operate the cooler without the tilt.

We use a photonic approach to meet these stringent demands of selective thermal emission in the mid-infrared, and strong solar reflection. An extensive numerical optimization scheme (see Methods) is used to achieve the photonic design schematically shown in Fig. 1d with a scanning electron microscope cross-section. The photonic radiative cooler consists of seven alternating layers of hafnium dioxide (HfO_2) and silicon dioxide (SiO_2) of varying thicknesses, on top of 200 nm of silver (Ag), which are all deposited on top of a 200-mm silicon wafer. The bottom four layers of HfO_2 and SiO_2 have thicknesses that are less than 100 nm and assist in optimizing solar reflection in a manner akin to that achievable using periodic one-dimensional photonic crystals. HfO_2 serves as a high-index material that also presents low ultraviolet absorption, a useful feature when optimizing for solar reflectance, while SiO_2 is optically transparent and is the low-index layer. The use of HfO_2 is, however, not essential, and can be replaced with titanium dioxide (TiO_2), which is less expensive. The top three layers are much thicker and are primarily responsible for thermal radiation from the cooler,

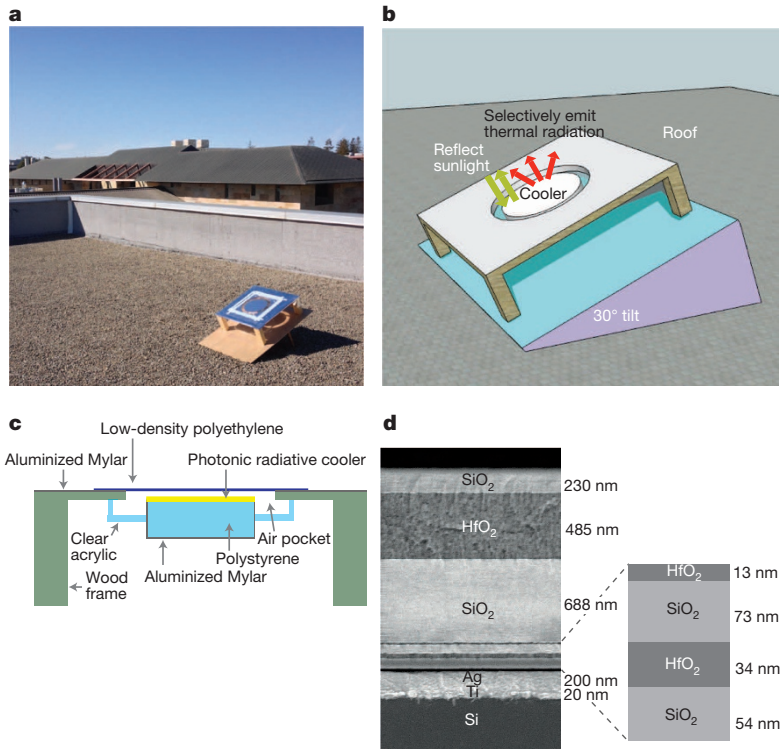

Figure 1 | Rooftop apparatus and photonic radiative cooler. **a**, Photo of the apparatus and radiative cooler on the test rooftop in Stanford, California. **b**, Three-dimensional schematic of the apparatus and radiative cooler, showing the general mode of operation of the radiative cooler. The apparatus is designed to minimize conductive and convective heat exchange to the cooler. **c**, Cut-out schematic of the apparatus through the middle, showing how an air pocket is created around the radiative cooler. Surfaces adjacent to this air pocket heat up minimally due to incident solar irradiance and therefore minimize the heat load on the air inside the pocket. Mylar is polyethylene terephthalate. **d**, Scanning electron microscope image of the photonic radiative cooler that is designed, implemented and tested in our experiments. It consists of seven layers of HfO_2 and SiO_2, whose thicknesses are defined by extensive numerical optimization (see Methods), on top of 200 nm of Ag, a 20-nm-thick Ti adhesion layer, and a 750-μm-thick, 200-mm-diameter Si wafer substrate.

through a combination of material properties and interference effects. SiO_2 has a strong peak in its absorptivity near 9 μm due to its phonon–polariton resonance. HfO_2 also presents non-zero absorption and hence emission in the 8–13 μm wavelength range[28]. The combination of all these layers results in a macroscopically planar and integrated structure that collectively achieves high solar reflectance and strong thermal emission.

The photonic radiative cooler's absorptivity/emissivity spectrum is experimentally characterized and shown in Fig. 2. The cooler shows minimal absorption when integrated from 300 nm to 4 μm, where the solar spectrum is present, in Fig. 2a, reflecting 97% of incident solar power at near-normal incidence. In Fig. 2b we observe that the cooler has strong and remarkably selective emissivity in the atmospheric window between 8 μm and 13 μm. Moreover, the photonic radiative cooler's thermal emissivity persists to large angles (see Extended Data Fig. 1), a useful feature to maximize radiated power P_{rad}, a hemispherically integrated quantity—see equation (2)—and reminiscent of the behaviour of hyperbolic metamaterials[29]. Photonic design fundamentally enables these spectral properties, which in turn are essential to achieving below-ambient radiative cooling. This spectral behaviour, and below-ambient cooling, is not achievable using these materials individually with conventional metallic reflectors.

We demonstrate the performance of the photonic radiative cooler on a clear winter day in Stanford, California, by exposing it to the sky on a building roof during daylight hours and comparing its steady-state temperature to the ambient air temperature. As shown in the temperature data of Fig. 3a, immediately after the sample is exposed to the environment (shortly before 10:00 local time in Fig. 3a), its temperature drops to approximately 4° to 5° Celsius below the ambient air temperature, even though significant solar irradiance is already incident on the sample. This is a key signature of radiative cooling, and a counterintuitive result during the day: we typically think of surfaces increasing their temperature when removed from the shade and exposed to the Sun during the day. We observe the photonic radiative cooler's temperature for over five hours under direct sunlight. Over 800 W m^{-2} of solar power is incident on the sample for three of the five hours. The cooler maintains a steady-state temperature substantially below the air temperature over the entire day, and is 4.9°C ± 0.15°C below the air temperature between 13:00 and 14:00 (local time) when the solar irradiance is in the range 800–870 W m^{-2}. To illustrate the significance of this result, we compare in Fig. 3b the photonic radiative cooler's performance against 200-mm wafers in identical apparatuses coated with conventional materials: carbon black paint and aluminium. The black paint reaches near 80° C, which is more than 60 °C above the ambient air temperature, while the aluminium reaches nearly 40° C, which is 20° C above the ambient air temperature. Typical roofing material has strong solar absorption and hence significantly heats up under direct sunlight, as emulated by the black paint result here. Also, one still sees very strong heating with an aluminium film, even though it provides relatively strong solar reflection.

We next characterize the photonic radiative cooler's cooling power. We allow its temperature to reach the previously achieved steady-state value under peak sunlight conditions of nearly 900 W m^{-2}. We then input heat to the cooler in steps over the course of one hour and observed

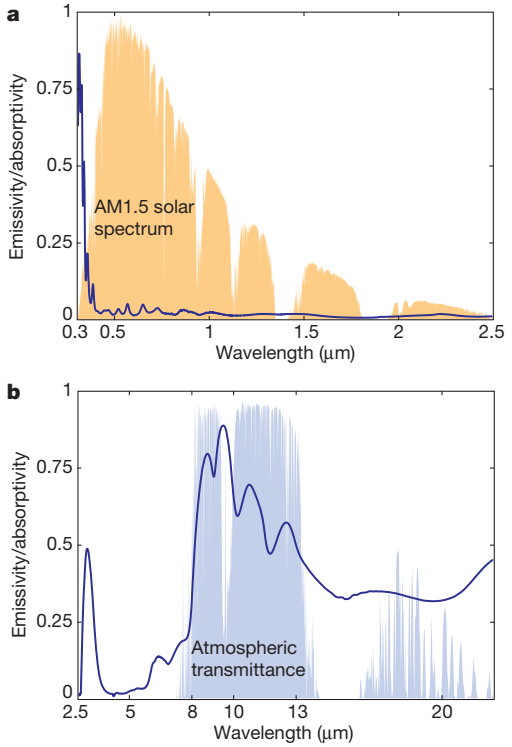

Figure 2 | Emissivity/absorptivity of the photonic radiative cooler from the ultraviolet to the mid-infrared. **a**, Measured emissivity/absorptivity at 5° angle of incidence of the photonic radiative cooler over optical and near-infrared wavelengths using an unpolarized light source, with the AM1.5 solar spectrum plotted for reference. The cooler reflects 97% of incident solar radiation. **b**, Measured emissivity/absorptivity of the cooler at 5° angle of incidence over mid-infrared wavelengths using an unpolarized light source, with a realistic atmospheric transmittance model plotted for reference[26]. The photonic cooler achieves strong selective emission within the atmospheric window.

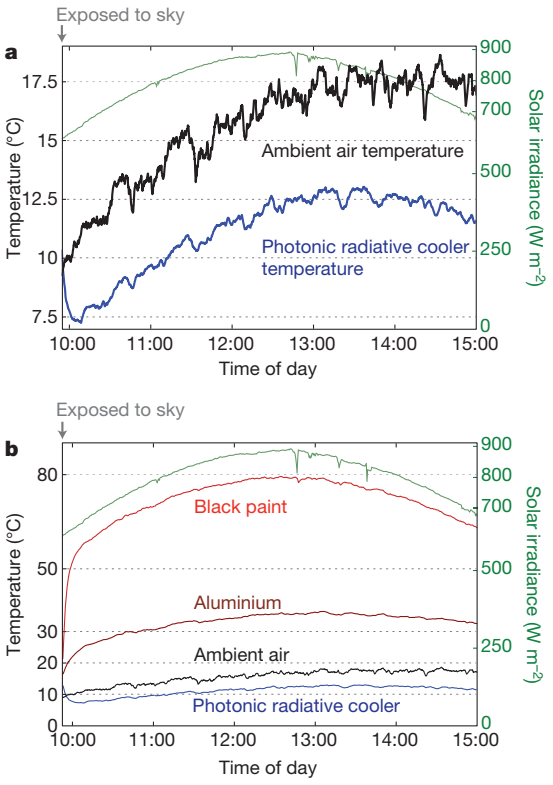

Figure 3 | Steady-state temperature of photonic radiative cooler. **a**, Rooftop measurement of the photonic radiative cooler's performance (blue) against ambient air temperature (black) on a clear winter day in Stanford, California. The photonic radiative cooler immediately drops below ambient once exposed to the sky, and achieves a steady-state temperature T_s of 4.9 °C ± 0.15 °C below ambient for over one hour where the solar irradiance incident on it (green) ranges from 800 W m^{-2} to 870 W m^{-2}. **b**, Comparing the photonic radiative cooler's performance against two reference roofing materials: black paint and aluminium. The paint reaches a temperature up to 80 °C, or 60 °C above ambient, while the aluminium reaches nearly 40 °C, or 20 °C above ambient. Only the photonic cooler stays well below ambient under direct solar irradiance.

the cooler's temperature at each step, as shown in Fig. 4a. With each increase of heat input, the temperature of the cooler rises to a new steady state. We plot the temperature of the cooler as a function of heat power in Fig. 4b. The temperature of the cooler reaches ambient temperature with an input heat power of 40.1 ± 4.1 W m^{-2}, indicating that substantial cooling power is available from this device. We next develop a theoretical model of our photonic cooler. This model is based on equation (1), where we use the spectral data of Fig. 2, as well as a model of the atmospheric transmittance[26] (see Methods), and a model for the conductive and convective losses of the apparatus, that together yield a value of $h_c = 6.9\ \mathrm{W\ m^{-2}\ K^{-1}}$ (see Methods and Extended Data Fig. 2). The theoretical model agrees excellently with the experimental data (Fig. 4b). The model can also be used to predict the steady-state temperature and power balance of the photonic radiative cooler as a function of time, and as compared against the observed performance of the sample under both daytime and night-time conditions (Extended Data Fig. 3). Moreover, the model indicates that lower steady-state temperatures can be reached by the cooler by reducing convective losses (see Methods). Under the same atmospheric and solar conditions, but with $h_c \to 0$, our device should achieve a steady-state temperature of 19.5 °C below ambient (see Extended Data Fig. 2c). Substantial gains in the photonic radiative cooler's performance are thus achievable by improved packaging alone.

The below-ambient cooling under peak daylight conditions shown here presents the possibility for purely passive, water-free approaches to cooling buildings and vehicles at all hours of the day. A preliminary analysis indicates that photonic radiative coolers could compete favourably in economic terms against other rooftop renewable energy options for cooling such as photovoltaic panels but may also work cooperatively with them (see Methods and Extended Data Fig. 4). A key engineering challenge will be to minimize parasitic heating of the radiative cooler from the surroundings while delivering the desired heat load to it efficiently. With the remarkable degree of spectral and thermal control made possible by photonic approaches, cooling power performance in favourable atmospheric conditions could be improved to more than 100 W m^{-2} (ref. 14). Improving building efficiency with a view towards reducing the need for active cooling has taken on renewed urgency on our warming planet, where the increase in carbon emissions caused by air conditioning is predicted to be faster than the decline in emissions from reduced heating[30]. In off-grid areas of the developing world, achieving radiative cooling during the daytime offers the opportunity to enable electricity-free cooling for critical needs like long-term food and medical supply storage. More broadly, our results point to the largely unexplored opportunity of using the cold darkness of the Universe as a fundamental renewable thermodynamic resource for improving energy efficiency here on Earth.

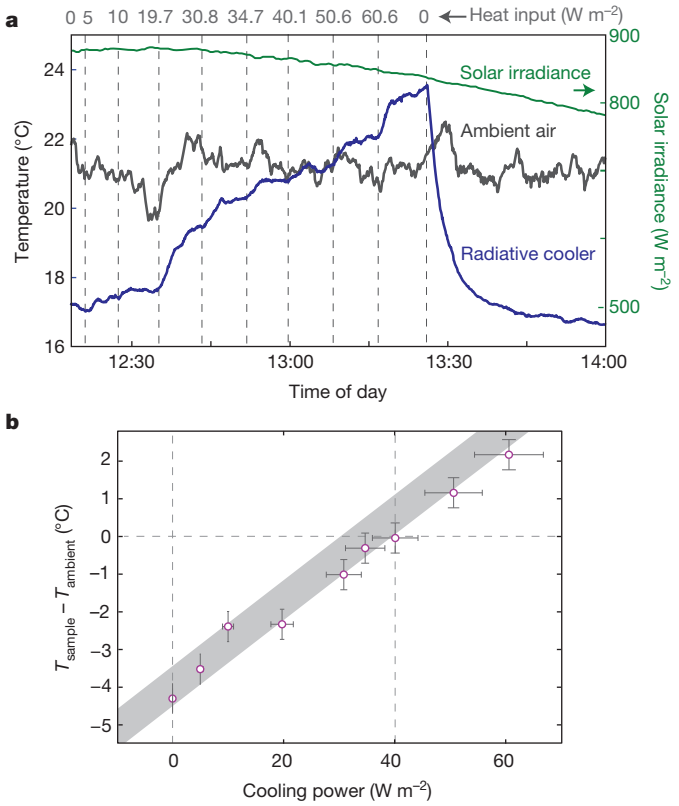

Figure 4 | Cooling power of photonic radiative cooler. **a**, Rooftop measurement of the photonic radiative cooler's temperature (blue), relative to ambient air temperature (black), in response to step-wise increasing inputs of heat (quantity shown at top at the beginning of each time period). For an input of 40.1 ± 4.1 W m^{-2} the radiative cooler reaches ambient air temperature, where solar irradiance of 860 W m^{-2} is incident on the cooler. **b**, The average temperature reached by the cooler over the last two minutes of each time period in **a** relative to ambient air temperature (T_{sample} minus $T_{ambient}$) for each associated value of input heat, with error bars defined by instrument and measurement error (see Methods). The predictions of a theoretical model for $h_c = 6.9\ \mathrm{W\ m^{-2}\ K^{-1}}$ are shown in the grey band, whose bounds are set by uncertainty associated with atmospheric transmittance.

Online Content Methods, along with any additional Extended Data display items and Source Data, are available in the online version of the paper; references unique to these sections appear only in the online paper.

Received 23 April; accepted 22 September 2014.

1. Kelso, J. K. (ed.) *2011 Buildings Energy Data Book* http://buildingsdatabook.eren.doe.gov/docs/DataBooks/2011_BEDB.pdf (US Department of Energy, Office of Energy Efficiency and Renewable Energy, 2011).
2. Trombe, F. Perspectives sur l'utilisation des rayonnements solaires et terrestres dans certaines régions du monde. *Revue Générale Thermique* **6,** 1285–1314 (1967).
3. Catalanotti, S. *et al.* The radiative cooling of selective surfaces. *Sol. Energy* **17,** 83–89 (1975).
4. Bartoli, B. *et al.* Nocturnal and diurnal performances of selective radiators. *Appl. Energy* **3,** 267–286 (1977).
5. Granqvist, C. G. & Hjortsberg, A. Surfaces for radiative cooling: silicon monoxide films on aluminum. *Appl. Phys. Lett.* **36,** 139–141 (1980).
6. Granqvist, C. G. & Hjortsberg, A. Radiative cooling to low temperatures: general considerations and application to selectively emitting SiO films. *J. Appl. Phys.* **52,** 4205–4220 (1981).
7. Berdahl, P., Martin, M. & Sakkal, F. Thermal performance of radiative cooling panels. *Int. J. Heat Mass Transf.* **26,** 871–880 (1983).
8. Berdahl, P. Radiative cooling with MgO and/or LiF layers. *Appl. Opt.* **23,** 370–372 (1984).
9. Orel, B., Gunde, M. & Krainer, A. Radiative cooling efficiency of white pigmented paints. *Sol. Energy* **50,** 477–482 (1993).
10. Gentle, A. R. & Smith, G. B. Radiative heat pumping from the earth using surface phonon resonant nanoparticles. *Nano Lett.* **10,** 373–379 (2010).
11. Gentle, A., Aguilar, J. & Smith, G. Optimized cool roofs: integrating albedo and thermal emittance with *R*-value. *Sol. Energy Mater. Sol. Cells* **95,** 3207–3215 (2011).
12. Nilsson, T. M. & Niklasson, G. A. Radiative cooling during the day: simulations and experiments on pigmented polyethylene cover foils. *Sol. Energy Mater. Sol. Cells* **37,** 93–118 (1995).
13. Nilsson, T. M., Niklasson, G. A. & Granqvist, C. G. A solar reflecting material for radiative cooling applications: ZnS pigmented polyethylene. *Sol. Energy Mater. Sol. Cells* **28,** 175–193 (1992).
14. Rephaeli, E., Raman, A. & Fan, S. Ultrabroadband photonic structures to achieve high-performance daytime radiative cooling. *Nano Lett.* **13,** 1457–1461 (2013).
15. Lin, S.-Y. *et al.* Enhancement and suppression of thermal emission by a three-dimensional photonic crystal. *Phys. Rev. B* **62,** R2243–R2246 (2000).
16. Greffet, J.-J. *et al.* Coherent emission of light by thermal sources. *Nature* **416,** 61–64 (2002).
17. Narayanaswamy, A. & Chen, G. Thermal emission control with one-dimensional metallodielectric photonic crystals. *Phys. Rev. B* **70,** 125101 (2004).
18. Luo, C., Narayanaswamy, A., Chen, G. & Joannopoulos, J. D. Thermal radiation from photonic crystals: a direct calculation. *Phys. Rev. Lett.* **93,** 213905 (2004).
19. Lee, B. J., Fu, C. J. & Zhang, Z. M. Coherent thermal emission from one-dimensional photonic crystals. *Appl. Phys. Lett.* **87,** 071904 (2005).
20. Drevillon, J. & Ben-Abdallah, P. Ab initio design of coherent thermal sources. *J. Appl. Phys.* **102,** 114305 (2007).
21. Schuller, J., Taubner, T. & Brongersma, M. Optical antenna thermal emitters. *Nature Photon.* **3,** 658–661 (2009).
22. Rephaeli, E. & Fan, S. Absorber and emitter for solar thermo-photovoltaic systems to achieve efficiency exceeding the Shockley-Queisser limit. *Opt. Express* **17,** 15145–15159 (2009).

23. Wu, C. *et al.* Metamaterial-based integrated plasmonic absorber/emitter for solar thermo-photovoltaic systems. *J. Opt.* **14,** 024005 (2012).
24. De Zoysa, M. *et al.* Conversion of broadband to narrowband thermal emission through energy recycling. *Nature Photon.* **6,** 535–539 (2012).
25. Lenert, A. *et al.* A nanophotonic solar thermophotovoltaic device. *Nature Nanotechnol.* **9,** 126–130 (2014).
26. Berk, A. *et al.* Modtran5: 2006 update. *Proc. SPIE* **6233,** 62331F (2006).
27. Martin, M. & Berdahl, P. Characteristics of infrared sky radiation in the United States. *Sol. Energy* **33,** 321–336 (1984).
28. Bright, T., Watjen, J., Zhang, Z., Muratore, C. & Voevodin, A. Optical properties of HfO_2 thin films deposited by magnetron sputtering: from the visible to the far-infrared. *Thin Solid Films* **520,** 6793–6802 (2012).
29. Jacob, Z. *et al.* Engineering photonic density of states using metamaterials. *Appl. Phys. B* **100,** 215–218 (2010).
30. Isaac, M. & van Vuuren, D. P. Modeling global residential sector energy demand for heating and air conditioning in the context of climate change. *Energy Policy* **37,** 507–521 (2009).

Acknowledgements This work is supported by the Advanced Research Projects Agency-Energy (ARPA-E), Department of Energy (contract number DE-AR0000316). We acknowledge discussions with J. Eaton and K. Goodson. Part of this work was performed at the Stanford Nanofabrication Facility, which is supported by the National Science Foundation through the NNIN under grant number ECS-9731293, and the Stanford Nano Center (SNC)/Stanford Nanocharacterization Laboratory (SNL), part of the Stanford Nano Shared Facilities.

Author Contributions A.P.R. and S.F. envisioned and implemented the experimental studies, and wrote the manuscript. A.P.R. and M.A.A. built and executed the rooftop experiments. A.P.R. designed and characterized the radiative cooler. L.Z. and E.R. provided technical support and conceptual advice.

Author Information Reprints and permissions information is available at www.nature.com/reprints. The authors declare no competing financial interests. Readers are welcome to comment on the online version of the paper. Correspondence and requests for materials should be addressed to A.P.R. (aaswath@stanford.edu) or S.F. (shanhui@stanford.edu).

METHODS

Photonic design optimization. The needle optimization method[31] is used to determine and optimize the number of layers and layer thicknesses of the photonic radiative cooler. The target metrics chosen for optimization were ideal reflectivity over the solar spectrum, weighted by the AM1.5 solar spectrum, and ideal emissivity in the range 8–13 μm. A combination of simulated annealing and quasi-newton methods are used to re-optimize layer thicknesses. Ag is defined to be the substrate layer, and HfO_2 and SiO_2 the materials to be used as alternating inserted layers. Refractive indices and extinction coefficients used in the optimization are derived from the ellipsometry of the bulk deposited layers of the materials for SiO_2 and Ag from 300 nm to 1,500 nm, with other values for other materials and wavelengths ranges coming from tabulated references[32].

Cooler fabrication and characterization. The photonic radiative cooler was deposited using electron beam evaporation on top of a 750-μm-thick, 200-mm-diameter silicon wafer by LGA Thin Films. A 20-nm-thick adhesion layer of Ti was first deposited, followed by 200 nm of Ag, and the seven alternating dielectric layers of HfO_2 and SiO_2 at the thicknesses shown in Fig. 1d. Thicknesses are monitored using a quartz crystal monitor during deposition. Depositing a thick layer of HfO_2 necessitates multiple cool-downs to prevent overheating due to the high temperatures needed for its evaporation. The reflectance of the cooler was characterized in the visible and near-infrared using a spectrophotometer (Jasco V-670) with an unpolarized light source and a calibrated high specular reflectance standard (Ocean Optics STAN-SSH), and is shown in Fig. 2a. In the infrared, a Fourier transform infrared spectrometer (Thermo Scientific Nicolet 6700) with an unpolarized light source is used to characterize the cooler's reflectance with a gold film used as a reflectance standard, as shown in Fig. 2b. A variable-angle accessory (Harrick Seagull) allows for reflectance measurements at varying angles of incidence from 5° to 85° (see Extended Data Fig. 1 for data). A scanning electron microscope (FEI Nova NanoSEM 450) is used to image the layers and is shown in Fig. 1d.

Rooftop measurement. The radiative cooler and reference materials were tested on the flat roof of a three-storey building (Fig. 1a) in Stanford, California, in mid-December 2013. The Sun's peak altitude was 30° above the horizon on the days testing occurred, while the apparatus containing the radiative coolers was placed on a platform tilted at $30° \pm 2°$. Thus at maximum solar irradiance $\theta_{Sun} = 30° \pm 2°$.

The apparatus containing the radiative cooler consists of a wood frame covered by a layer of aluminized Mylar. The top surface of the frame has a circular 10-inch aperture. A clear acrylic box with the top side open, and the bottom side containing a 200-mm aperture is joined and sealed to the underside of the wooden frame's top surface. An aluminized Mylar-coated polystyrene pedestal is then inserted through the acrylic box's 200-mm aperture, and the radiative cooler is placed on top of the polystyrene. A 12.5-μm-thick low-density polyethylene film is then used to seal the top aperture on the wooden frame, and serves as an infrared-transparent wind shield. This design, schematically represented in Fig. 1c, creates a well-sealed air pocket around the sample. Surfaces in contact with the air pocket absorb sunlight minimally and thus minimize the heat load on the sample due to external solar heating of adjacent surfaces and air.

The back-surface of the radiative cooler is instrumented with an adhesive resistance temperature detector sensor with ±0.15 °C accuracy mounted at the centre of the wafer, connected to a data logger (Omega OM-CP-OCTRTD). To determine the steady-state temperature, the entire apparatus is placed on the angled platform on the roof and shielded with an aluminium sheet, blocking access to the sky. The radiative cooler and apparatus are then exposed to the sky, and left on the roof through the course of the day. Next to the radiative cooler, we also expose reference samples of aluminium and carbon black paint to the sky, also mounted in the same apparatus design and platform. Direct and diffuse solar irradiance incident on the sample is measured over the same time period using a pyranometer (Kipp & Zonen CMP 6) and a data logger rated to a directional error of $\pm 20\ W\ m^{-2}$. The pyranometer is placed on the same tilted platform as the apparatus. Ambient air temperature is measured using an air-temperature resistance temperature detector probe with ±0.15° C accuracy in a sun-shaded area with free air flow near the sample, but outside the air pocket around the sample.

To determine the cooling power of the radiative cooler a circular 3.4-inch-diameter polyimide resistive heater is attached adhesively to the underside of the cooler. The heater delivers varying amounts of heat to varying input voltages from a direct-current (d.c.) power source (with ±1% readout accuracy), and has a resistance tolerance of ±10%. The temperature of the sample shown here represents the average temperature over the whole sample. The temperature distribution uncertainty is ±0.4° C, as determined by measurement and simulation. The range is represented as the uncertainty in Fig. 4b. In the experiment, the radiative cooler is initially allowed to equilibrate with zero heat input. Increasing quantities of heat are then applied constantly for time periods of 8–10 min, as shown in Fig. 4a. With each increase in heat applied, denoted numerically at the top of Fig. 4a, the temperature of the sample rises and plateaus. The average temperature over the last two minutes of each time block is used to define the radiative cooler's temperature for the corresponding heat input shown in Fig. 4b. Uncertainty in the reported cooling power is based on the propagation of instrument and resolution error. The solar irradiance on the radiative cooler over the entire time period of the cooling power experiment stays within a range of 850–880 $W\ m^{-2}$.

Theoretical model of cooler and apparatus. The theoretical model represented by the grey line in Fig. 4b is arrived at by using equation (1). Specifically, we input the experimentally derived absorption/emission data of the photonic cooler for the relevant angles of incidence (θ_{Sun} at optical wavelengths), the AM1.5 spectrum weighted to the net irradiance measured, and a model of the atmospheric transmittance. MODTRAN5 is used to model the atmosphere in the infrared for a clear sky at mid-latitudes during the winter[26]. The model accounts for the tilt of the apparatus and the presence of the thin polyethylene cover. Given a range of potential atmospheric conditions, we assign a ±5% uncertainty to this atmospheric model, which in turn defines the bounds of the grey line shown in Fig. 4b. h_c is derived by numerical heat transfer modelling (see below and Extended Data Fig. 2).

The theoretical model is also used to calculate the steady-state temperature of the photonic radiative cooler over the course of a day. Given the observed ambient air temperatures (averaged using a moving 30-min window) and solar irradiance from the day on which the Fig. 2 data was taken, in addition to the measured spectral emissivity of the photonic radiative cooler and atmospheric transmission from MODTRAN5, we solve equation (1) for T_s by a binary search and plot the result as a grey band in Extended Data Fig. 3a. The bounds of the grey band are defined by a range of values of h_c between $4\ W\ m^{-2}\ K^{-1}$ and $8\ W\ m^{-2}\ K^{-1}$, since h_c can vary over the course of a day given varying environmental conditions. The model matches the observed temperature of the photonic radiative cooler (blue line) quite well, indicating the utility of the model in predicting and characterizing the performance of a radiative cooler at any hour of the day and at any time of the year. In particular, the data from Fig. 2 is extended to show the performance of the photonic radiative cooler on the same day under night-time conditions in Extended Data Fig. 3a. Over approximately an hour, the Sun dips and sets beyond nearby hills, and solar irradiance incident on the photonic radiative cooler falls to nearly 0. As $P_{Sun} \rightarrow 0$, the photonic radiative cooler's performance improves, with a steady-state temperature approximately 7° C below ambient achieved (see Extended Data Fig. 3b). The model can also be used to break down the power balance of equation (1) into its constituent terms to better elucidate the contributions to the device's performance (see Extended Data Fig. 3c).

Heat-transfer modelling of experimental apparatus. Heat-transfer simulations were performed in COMSOL in order to better understand convective and conductive loss mechanisms in the experiment, and to quantify $P_{cond+conv}$ and h_c as defined in equation (5). The numerical model simulates the experimental setup in two dimensions with three objects: a thin radiator, surrounding air and the supporting polystyrene block. We define the air temperature and the conductive properties of all objects and the value of the heat flux P_{out} that is leaving the radiator, allowing us to infer $P_{cond+conv}$ as a function of the radiator's temperature T. The outside boundaries of the system (shown at the top of Extended Data Fig. 2a) are set to the air temperature. The simulation handles the fluid mechanics in the air pocket and the conduction in the polystyrene block and the radiator in order to determine the steady-state temperature T of the sample for each value of P_{out}. At the steady-state temperature, $P_{out} = P_{cond+conv} = Ah_c(T_{amb} - T)$.

The result of this simulation is shown in Extended Data Fig. 2b as the blue line, whose slope is the simulation's prediction of the non-radiative heat transfer coefficient h_c. By linear regression we find a value of $h_c = 6.9\ W\ m^{-2}\ K^{-1}$ which is subsequently used with the theoretical model in Fig. 4b and fits the observed data very well.

As a reference we also plot the net radiated power of the radiative cooler $P_{net}(T, T_{amb}) = P_{rad}(T) - P_{atm}(T_{amb}) - P_{Sun}$, in Extended Data Fig. 2b. Since P_{net} cannot be independently experimentally obtained, we use the theoretical model previously discussed. As a check, the intersection of these curves is the prediction of the theoretical model and numerical heat transfer simulation for the expected steady-state temperature T_s of the photonic radiative cooler in the apparatus. We find a value of 4.2 °C below ambient, agreeing quite well with our experimental result of 4.3 °C below ambient in Fig. 4b for the data obtained during the day when cooling power is measured (a different day from the day on which the steady-state temperature was measured). The combination of a theoretical model based on radiative properties, and a numerical heat transfer model for non-radiative behaviour, can thus model the experimental behaviour of the photonic radiative cooler remarkably well.

Building-level energy saving analysis. We assess the energy savings enabled by covering the roof of a typical commercial building with the photonic radiative cooler in a rudimentary way, and project the levelized (accounting for the lifetime of an installation and the discount rate) cost of cooling for a range of installed costs. To highlight the fundamental arguments for energy savings with our radiative cooling

strategy, we perform a basic analysis, in which we assume that the building has a mechanism to transfer part of the heat load to the radiating surface on the roof, while a standard heating, ventilation and air conditioning (HVAC) system handles other cooling requirements. *EnergyPlus* simulations[33] are used to determine the cooling load for a three-story medium-sized commercial benchmark building[34] with a 1,600 m^2 roof on an hourly basis over a year in Phoenix, Arizona, USA. The building's interior is assumed to be maintained at $T_{interior} = 24\,^{\circ}C$ at all hours. The cooling power made available by the photonic radiative cooler is then calculated on an hourly basis, $P_{cool}(T = T_{interior}, T_{amb}(t), t)$, from equation (1). Typical Meteorological Year (TMY2) data[35] for Phoenix is used to determine $T_{amb}(t)$ and $P_{Sun}(t)$ on an hourly basis. The model of the photonic radiative cooler discussed in the main paper is used to calculate P_{cool} on an hourly basis for each corresponding value of T_{amb} and P_{Sun} at the specified $T = T_{interior}$ set point.

In our analysis, these hourly values of P_{cool} are then subtracted from the heat load for the building as determined by the *EnergyPlus* simulations. The remaining heat load is assumed to be dissipated with a standard cooling system with a coefficient of performance of 2.8 (ref. 34). Therefore, the use of a photonic radiative cooler translates into a savings in electric power of P_{cool} divided by the coefficient of performance. Integration of this savings over a period of time then gives overall electricity savings in kilowatt hours. Here we take into account that the cooler can operate 24 h a day—the cooler in fact performs even better in the absence of sunlight than in the daytime. If there is minimal cooling demand for the building, for example during summer nights, the cooling power of the roof is pessimistically assumed to be unused. The resulting saving in kilowatt hours is plotted in Extended Data Fig. 4 on a monthly basis, and yields an annual projected electricity saving of 1.185×10^5 kWh. By being able to operate at all hours of the day, photonic radiative coolers will have shorter payback periods for buildings and regions where there is cooling demand at all hours. This can be seen in Extended Data Fig. 4, with more kilowatt hours saved during summer months in Phoenix when, in addition to higher demand during the day, there is cooling demand even at night.

To provide a rough estimate of the monetary value of the energy savings made possible by the photonic radiative cooling we perform a standard project finance analysis. We assume a twenty-year lifespan, grid electricity cost of $\$0.10\,kWh^{-1}$, fix operating costs at $\$0.8\,m^{-2}$ (between 1% and 2% of the range of installed costs[36]), a discount rate of 5% and consider a range of installed costs of between $\$20\,m^{-2}$ and $\$70\,m^{-2}$. Such installed costs are in line with what is currently achieved at scale for similar multilayer coatings for low-emissivity windows[37] and other surfaces. This analysis then yields unsubsidized levelized costs of cooling (for the energy saved) between $\$0.03\,kWh^{-1}$ and $\$0.09\,kWh^{-1}$, which are below aggressive levelized cost projections for both rooftop and utility-scale photovoltaics over the coming decade[38]. This indicates that photonic radiative coolers could potentially be an attractive large-area renewable solution to reducing cooling costs for buildings. They may also work cooperatively with rooftop photovoltaic systems based on a building's needs and energy use profile.

This simple analysis is meant to provide a first-order estimation of the potential of photonic radiative coolers that operate at all hours of the day. We have not accounted for heat-transfer mechanisms to the radiative cooling panels themselves. In practice, the specific implementation and integration of radiative cooler systems may take different forms, including their direct integration with chillers and HVAC systems. Finally, we note that we assume the sunlight, almost all of which is reflected by our photonic radiative cooler, goes unused. Future designs and configurations may find ways of using this reflected sunlight, enabling shorter payback periods and lower levelized costs.

31. Tikhonravov, A. V., Trubetskov, M. K. & DeBell, G. W. Application of the needle optimization technique to the design of optical coatings. *Appl. Opt.* **35,** 5493–5508 (1996).
32. Palik, E. *Handbook of Optical Constants of Solids* (Academic Press Handbook Series, Elsevier Science & Tech, 1985).
33. Crawley, D. B., Pedersen, C. O., Lawrie, L. K. & Winkelmann, F. C. Energyplus: Energy simulation program. *ASHRAE J.* **42,** 49–56 (2000).
34. Deru, M. *et al.* US Department of Energy commercial reference building models of the national building stock. Tech. Rep. NREL/TP-5500-46861, http://www.nrel.gov/docs/fy11osti/46861.pdf (National Renewable Energy Laboratory, 2011).
35. Marion, W. & Urban, K. User's manual for TMY2s. Tech. Rep. http://rredc.nrel.gov/solar/pubs/tmy2/PDFs/tmy2man.pdf (National Renewable Energy Laboratory, 1995).
36. Campbell, M. Charting the progress of PV power plant energy generating costs to unsubsidized levels, introducing the PV-LCOE framework. In *Proc. 26th Eur. Photovoltaic Solar Energy Conf. (Hamburg)* 4409–4419 (2011).
37. Keshner, M. S. & Arya, R. R. Study of potential cost reductions resulting from super-large-scale manufacturing of PV modules. Tech. Rep., Final Subcontract Report NREL/SR-520–36846 (National Renewable Energy Laboratory, 2004).
38. Bazilian, M. *et al.* Re-considering the economics of photovoltaic power. *Renew. Energy* **53,** 329–338 (2013).

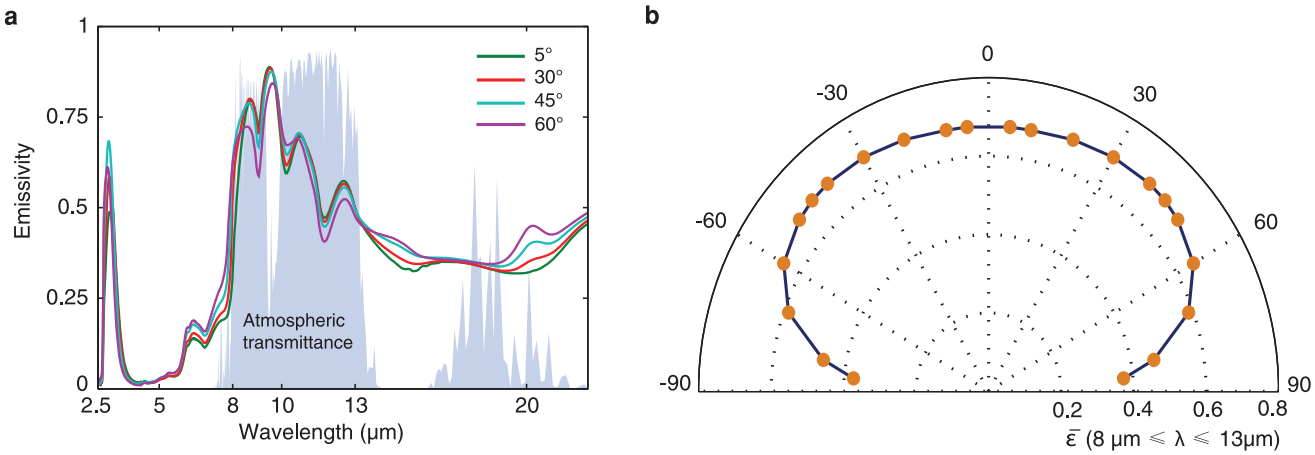

Extended Data Figure 1 | Angular emissivity of photonic radiative cooler. **a**, Measured emissivity/absorptivity of the cooler for variable angles of incidence over near- and mid-infrared wavelengths with a realistic atmospheric transmittance model plotted for reference[26]. **b**, Average measured emissivity $\bar{\varepsilon}$ of the photonic radiative cooler between 8 μm and 13 μm (the atmospheric transparency window) plotted as a function of polar angle of incidence. The cooler's emissivity within the window remains relatively constant between 5° and 60°, and remains high even at remarkably large angles of incidence, reminiscent of the behaviour of hyperbolic metamaterials.

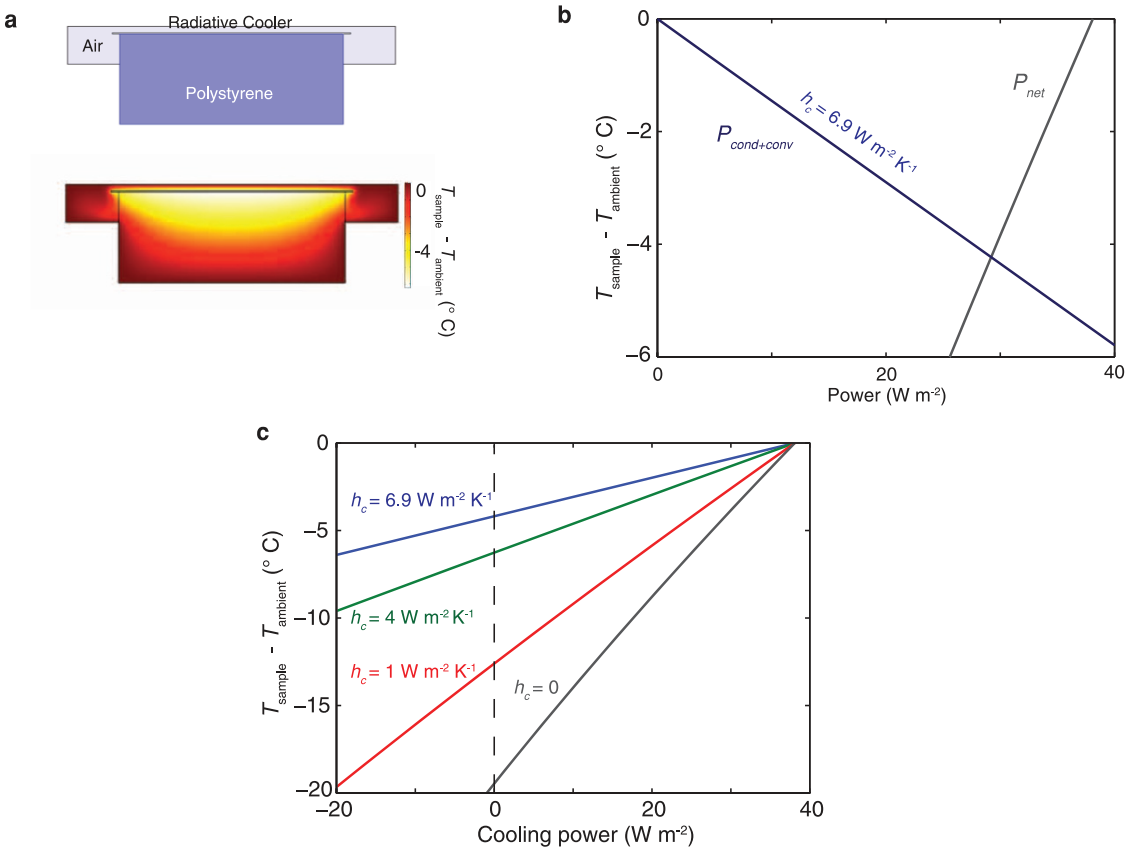

Extended Data Figure 2 | Numerical modelling of non-radiative heat exchange. **a**, A numerical simulation of the apparatus and radiative cooler (layout shown at top) yields a temperature distribution ($T_{sample} - T_{ambient}$) (bottom) within the geometry that takes into account non-radiative heat exchange in the apparatus. **b**, The simulation calculation for $P_{cond+conv}$ as a function of $T_{sample} - T_{ambient}$ (blue line) yields a value of $h_c = 6.9\ W\ m^{-2}\ K^{-1}$, which we use in our theoretical model to compare against experimental data in Fig. 4b. We also plot the theoretical model of net radiated power P_{net} that is based on the absorption/emission of the photonic radiative cooler (grey line). The intersection represents the predicted value of T_s of the photonic radiative cooler in this apparatus, and matches well our observed experimental value of $T_s = 4.3\ ^\circ C$ below ambient in Fig. 4b. **c**, Theoretical model plotted for various values of h_c. As $h_c \rightarrow 0$ the model predicts T_s of nearly 20 °C below ambient can be achieved by the photonic radiative cooler.

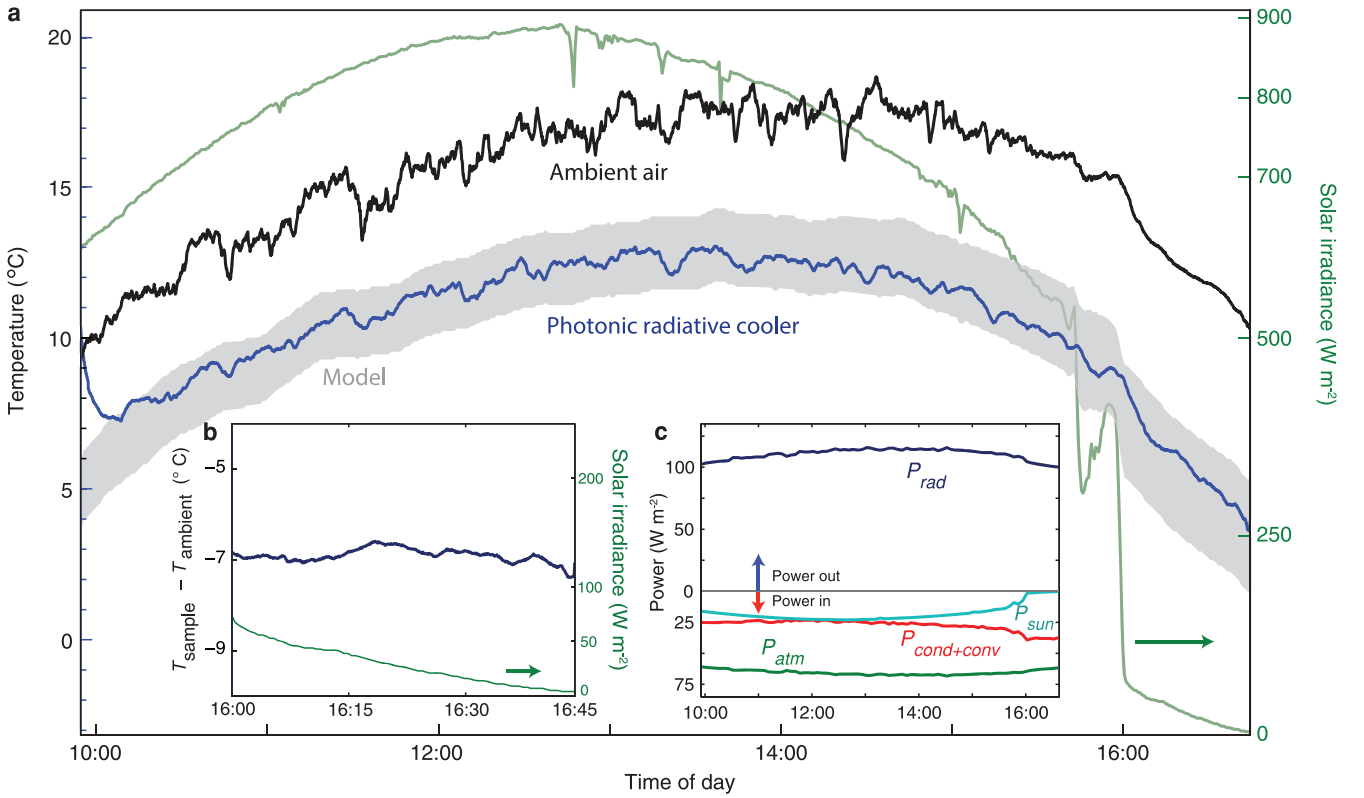

Extended Data Figure 3 | Modelling steady-state temperature under daytime and night-time conditions. **a**, The theoretical model is used to calculate the steady-state temperature of the photonic radiative cooler (see Methods) given observed air temperatures, solar irradiance and a range of values of h_c from 4 W m^{-2} K^{-1} to 8 W m^{-2} K^{-1} (grey band). The model is able to predict well the observed performance of the photonic radiative cooler through the course of the day (blue line, extending the data from Fig. 2) under both direct solar irradiance (green line) and when the Sun sets behind nearby hills, reducing irradiance to near-zero values. **b**, Data from this latter time period (effectively night-time conditions). As expected, the photonic cooler performs even better under no solar irradiance, with $T_{sample} - T_{ambient}$ of approximately 7 °C below ambient achieved. **c**, The four terms on the right hand side of equation (1) are plotted, using the model at T_s as a function of time, to elucidate the impact of each component on performance.

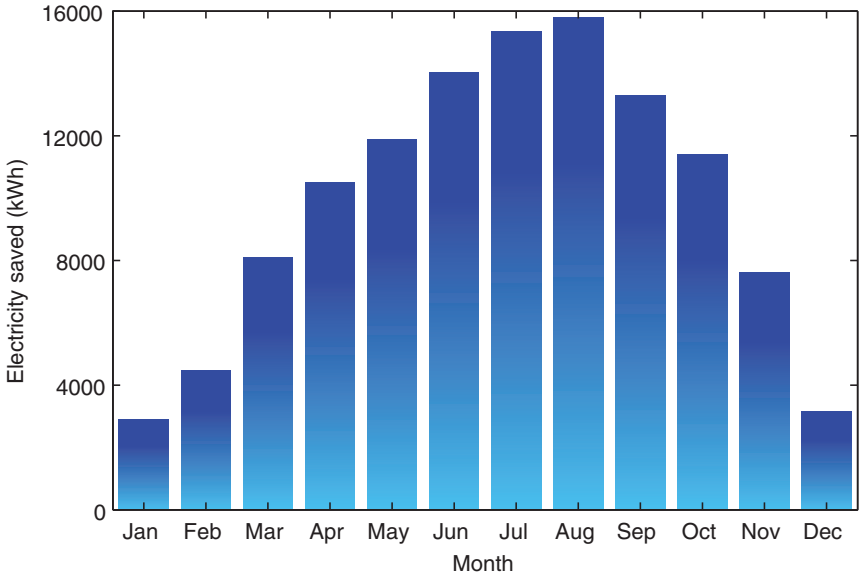

Extended Data Figure 4 | Energy savings for a medium commercial reference building with photonic radiative coolers. We use a simple approach to estimate the energy savings for the National Renewable Energy Laboratory three-story commercial benchmark building[31], assuming its 1,600 m^2 roof is covered with the photonic radiative cooler, and heat from its interior is transferred to the radiative panels (see Methods). Using the model of our photonic radiative cooler, the thermal cooling power of the radiative cooler is set relative to ambient air temperature and solar irradiance for Phoenix, Arizona, over a typical year (TMY2 data), and with an interior air temperature of 24° C. *EnergyPlus* simulations determine the cooling load the building places on the air-conditioning units (which is assumed to have a coefficient of performance of 2.8). The calculated cooling power of the radiative cooler is then subtracted from the thermal load on an hourly basis for the year, and electricity savings are subsequently inferred and plotted. Although this is a rudimentary analysis, it does indicate that more kilowatt hours are saved in summer months where there is greater cooling demand, and that the scale of the potential annual savings (1.185×10^5 kWh) is substantial.